BIOACTIVE SiC-BIOGLASS COMPOSITE THROUGH AN ALKALI-ACTIVATION OF THE SiO_2 NATIVE SILICA OXIDIZED LAYER

Guido Manuel OLVERA DE LA TORRE [1], Martin MICHALEK[2], Anna JUROVA[3], Gianmarco TAVERI[1,3,*]

[1]*Centre for Advanced Materials and Applications (CEMEA), Slovak Academy of Sciences (SAV), Dubravská cesta 9, Bratislava, Slovakia*

[2]*FunGlass, Alexander Dubček University of Trenčín, 911 50 Trenčín, Slovakia.*

[3]*Institute of Inorganic Chemistry (ICC), Slovak Academy of Sciences (SAS), Dubravská cesta 9, Bratislava, Slovakia*

[*]*Corresponding author: Gianmarco Taveri (gianmarco.taveri@savba.sk)*

Abstract: *Traditional Bioglass 45S5 is highly bioactive but mechanically fragile. While adding SiC (silicon carbide) can reinforce the material, standard high-temperature sintering often causes the glass to crystallize, which severely reduces its bioactivity. This work introduces a low-temperature alkali-activation technique to bypass these thermal issues. By reacting the native SiO_2 layer on SiC particles with a specific chemical activator, researchers synthesized a composite that mimics 45S5 bioglass composition under mild calcination. SEM-EDX and XRD confirmed a homogeneous matrix with a partial precipitation of combeite, a phase consistent with bioactive glass. TG-DTA confirmed the matrix undergoes a true glass transition before crystallization. Both the "green" and calcined samples remained highly bioactive, forming hydroxyapatite within one week of SBF immersion. This study proves that alkali-activation can effectively integrate hard ceramics into bioactive composites, creating a path for mechanically strong, highly reactive bone implants without the drawbacks of high-temperature processing.*

Keywords: *SiC; Glass-ceramics; Bio-activity; Bioceramics; Alkali-activation*

1. Introduction

The repair and replacement of bone tissue damaged by trauma, disease, or surgical resection constitutes one of the principal challenges in modern regenerative medicine. Autologous bone grafts remain the clinical gold standard, yet their use is constrained by donor-site morbidity, limited availability, and the risk of infection [1]. These limitations have driven sustained interest in synthetic bioactive materials capable of bonding chemically to living bone and stimulating osteoconduction. Among all synthetic alternatives, bioactive glasses occupy a privileged position owing to their unique ability to form a biologically active hydroxyapatite (HA) surface layer when exposed to physiological fluids, thereby establishing a direct bond with host bone tissue [2].

Bioglass 45S5, discovered by Hench et al. in 1971, was the first synthetic material demonstrated to bond to bone and is still the most clinically employed bioactive glass composition [3]. Its composition (45 wt.% SiO_2, 24.5 wt.% Na_2O, 24.5 wt.% CaO, and 6 wt.% P_2O_5) yields a highly disrupted silicate network with a low degree of polymerization, conferring exceptional ion release kinetics and bioactivity [4]. Upon immersion in simulated body fluid (SBF), 45S5 undergoes a well-established sequence of surface reactions: rapid ion exchange of Na^+ and Ca^{2+} with H^+ from solution, condensation of a silica-rich gel layer, followed by crystallization of a carbonate-substituted HA layer that is biochemically equivalent to bone mineral [5]. Despite this unrivalled bioactivity, the intrinsic brittleness and low fracture toughness of 45S5 glass (K_{IC} ~ 0.7–1.0 $MPa \cdot m^{1/2}$) severely restrict its application to non-load-bearing skeletal sites, making it unsuitable for trabecular or cortical bone substitution under mechanical loading [6].

A widely investigated strategy to overcome these mechanical limitations consists of the fabrication of bioactive glass-ceramic composites, in which a stiff and tough second phase reinforces the glassy matrix while ideally preserving or even enhancing its surface bioactivity. Alumina, zirconia, titania,

hydroxyapatite, and, more recently, silicon carbide (SiC) have all been explored as fillers for bioglass-based composites [7,8]. Among these reinforcements, SiC holds particular promise owing to its exceptional combination of high elastic modulus (~420 GPa), hardness, chemical inertness, and biocompatibility, as well as its native surface oxide layer (SiO_2) that offers a chemically reactive interface [9]. Silicon carbide is also regarded as a biocompatible ceramic: in vitro and in vivo studies have demonstrated that SiC particles and coatings do not elicit adverse inflammatory or cytotoxic responses in osteoblastic cell lines or animal models [10,11].

The state-of-the-art of SiC-bioglass composites, however, is burdened by a fundamental processing paradox. Conventional powder metallurgy routes (hot pressing, spark plasma sintering (SPS), or pressureless sintering) require temperatures above 900–1100°C to achieve adequate densification of a SiC-containing body [12]. At these temperatures, 45S5 bioglass undergoes extensive crystallization, primarily into combeite ($Na_2Ca_2Si_3O_9$) and wollastonite, which dramatically reduces the density of non-bridging oxygens and thus the ion release rate, severely impairing bioactivity [13]. Furthermore, the reducing atmosphere required to prevent SiC oxidation during sintering is thermodynamically incompatible with the network-modifier chemistry of 45S5 [14]. Several groups have attempted to circumvent this dilemma. Gonzalez et al. investigated the co-sintering of SiC particles in bioglass-ceramic matrices, reporting improved fracture toughness but substantial crystallization and reduced in vitro HA formation [15]. Leenakul et al. proved that high sintering temperatures are detrimental to the bioglass bioactivity [16]. Attempts using sol-gel derived glasses have extended processing windows somewhat, but the challenge of achieving intimate filler-matrix bonding without resorting to high-temperature densification remains unresolved [17].

Alkali-activation is a low-temperature inorganic binder technology in which an aluminosilicate or silica-rich precursor is dissolved and repolymerized into a three-dimensional amorphous or semi-crystalline gel network by reaction with a concentrated alkali hydroxide or silicate solution [18]. The resulting alkali-activated materials (AAMs) are processed at temperatures typically below 80–200°C, exhibit high compressive strengths, chemical durability, and are amenable to a wide variety of solid precursors. Recent work has demonstrated that the alkali-activation framework can be transposed to biomedical applications: alkali-activated metakaolin and fly-ash-based geopolymers have been evaluated as bone cements and scaffolds, with encouraging biocompatibility results [19,20]. Critically for the present application, the native SiO_2 layer invariably present on SiC particle surfaces is itself a reactive silica source. When SiC is pre-oxidized in air, the thickness of this layer can be tailored and quantified, providing a controllable amount of amorphous SiO_2 that can serve as the silicate precursor for in-situ alkali-activation. By stoichiometrically matching the dissolved silica with sodium hydroxide, calcium hydroxide, and phosphoric acid to reproduce the Bioglass 45S5 molar composition, it is in principle possible to grow a bioglass-precursor matrix directly on and between the SiC particles without any high-temperature densification step.

Here, we present the first application of alkali-activation chemistry to the synthesis of a SiC-bioglass composite. β-SiC powder is pre-calcined in air at 900°C to generate a controlled SiO_2 surface layer, which is subsequently activated with NaOH to form an in-situ sodium silicate binder. Stoichiometric additions of $Ca(OH)_2$ and H_3PO_4 complete the Bioglass 45S5 target composition. The composite green body is consolidated at a mild calcination temperature of 600°C, well below the crystallization onset of 45S5, to dehydrate the binder network. Microstructural, thermal, phase-compositional, and in vitro bioactivity assessments are reported and discussed in the context of the processing-structure-bioactivity relationship of this novel composite system.

2. Materials and methods

The reagents used for slurry preparation and processing of the alkali-activated material (AAM) comprised β-silicon carbide (SiC; >98 wt.% purity, D_{50} = 0.5 μm, oxygen content <1.0 wt.%, Superior Graphite, Japan), sodium hydroxide (NaOH) pellets serving as the alkaline activator (98% purity, Sigma Aldrich, USA), calcium hydroxide ($Ca(OH)_2$) powder (>95% purity, Sigma Aldrich, USA), phosphoric acid (H_3PO_4) solution (85 wt.% in H_2O, Sigma Aldrich, USA), and distilled water. Firstly, the SiC powder was calcined in air at 900 °C for one hour to thicken the oxidized layer on the particle's surface. Under these conditions, an O_2 content of 10 wt.% is achieved, measured by an O_2-analyzer (Horiba EMGA-830 analyzer, Horiba, Japan). Based on the equivalent amount of formed SiO_2 (approximately 19 wt.%), an amount of NaOH pellets was dissolved in water (concentration 1M) and kept under vigorous stirring. After complete dissolution, the calcined SiC was added to the solution to form a suspension, which was kept under stirring and heating (50 °C) for 3 hours to ensure the reaction of NaOH and SiO_2 into sodium silicate hydrate. Subsequently, the H_3PO_4 and $Ca(OH)_2$ were added to the suspension. The suspension was kept under stirring at 70 °C to let the water evaporate until the suspension became a thick slurry (having a solid-to-liquid ratio of approximately 0.5 measured by weighing a small wet droplet and then again after drying at 150°C for 30 minutes). The amount of each chemical was chosen to produce a stoichiometric Bioglass45S5 composition (SiO_2 45.0 wt.%, Na_2O 24.5 wt.%, CaO 24.5 wt.%, P_2O_5 6 wt.%). The paste was then cast in a plastic container and left to dry overnight at 60 °C, and then further dried at 150°C for 1 h. The so-produced green body (denoted SiCB45S5_AA) was then ready for further analysis. For the production of the calcined sample (SiCB45S5_600), the green body was placed in a furnace and heated in air at 600°C for 1 h (heating and cooling rate 10°C/min). The calcination was performed using alumina crucibles in a Clasic 0213 T furnace equipped with a Clasic Clare 4.0 controller (Clasic CZ s.r.o., Řevnice, Czechia).

An Empyrean Malvern X-ray diffractometer (Empyrean, Malvern Panalytical, UK) was used to measure the phase composition of the SiCB45S5_AA and SiCB45S5_600 samples, with the following parameters: Cu Kα radiation, λ = 1.5406 Å, 2θ = 10–70°, step-size 0.026°, counting time 50 s per step. The morphology of the microstructure was inspected through scanning electron microscopy (SEM) using a JEOL EVO 40 series electron microscope (JEOL, Japan), equipped with detectors for backscattered electrons and X-rays. Thermal behavior was analyzed by TGA/DTA in air to 800 °C at 10 °C/min, using an STA 449 F3 Jupiter (Netzsch Gerätebau GmbH, Germany). Disposable alumina crucibles were used for the measurements. The in vitro bioactivity assay was performed by immersing the samples in simulated body fluid (SBF) prepared according to the Kokubo method [21]. During soaking, the SBF amount (approx. 28 ml) was contained in sterile plastic containers. The containers were sealed and placed in an incubator (Binder Model B28, Binder GmbH, Tuttlingen, Germany) maintained at a constant temperature of 36.5 °C for 7 days. After the test, the samples were rinsed with ultrapure water and dried at room temperature in a desiccator. The formation of apatite layers on the sample surfaces was analyzed using SEM.

3. Results and discussions

3.1. Materials characterization

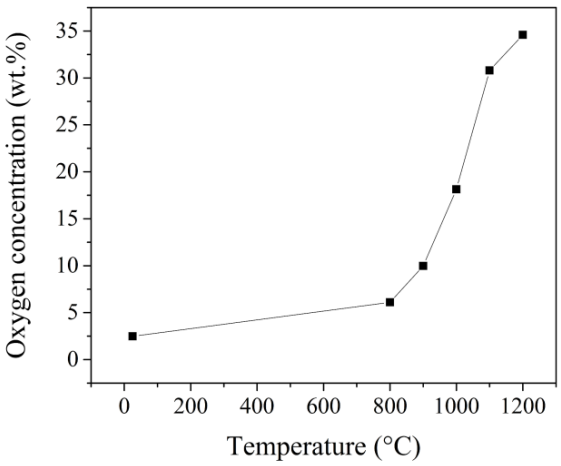

Figure 1. O_2 concentration (wt.%) measured through the O_2 material Analyzer of the SiC powder as a function of the calcination temperature.

The pre-calcination of β-SiC powder in air is a prerequisite for the alkali-activation route, as it generates the reactive SiO_2 surface layer required for in-situ sodium silicate formation. As shown in Figure 1, the oxygen content of the SiC powder increases monotonically with calcination temperature, reaching approximately 10 wt.% after treatment at 900 °C for 1 h. This behavior is consistent with the passive oxidation regime of SiC, in which the Deal-Grove parabolic oxidation model governs the growth of the amorphous SiO_2 scale at temperatures between 800 and 1200 °C [22]. The measured oxygen content of 10 wt.% at 900 °C corresponds, on a stoichiometric basis, to approximately 19 wt.% of amorphous SiO_2 per unit mass of powder, which provides the silica source for the alkali-activation reaction. Critically, the 900°C treatment was selected to maximize the available reactive silica while avoiding the onset of β- to α-SiC polytypic transformation and excessive SiO_2 layer thickness, which could impair dissolution kinetics during activation [23].

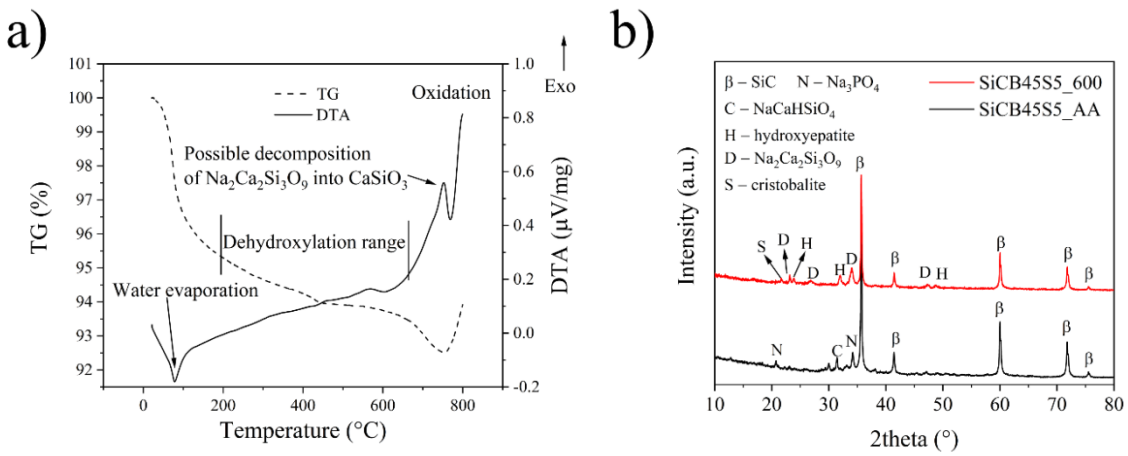

Figure 2. a) TG-DTA thermal analysis of the alkali-activated green-body (SiCB45S5_AA) sample in the temperature range of 25-800°C (heating rate 10°/min). b) XRD patterns of both alkali-activated green-body and the material calcined at 600°C (SiCB45S5_600).

The thermal behavior of the alkali-activated green body (SiCB45S5_AA) and its phase evolution upon calcination are reported in Figure 2. The TG-DTA trace (Figure 2a) reveals two distinct mass-loss events below 600°C. The first, a broad endothermic event centered around 100–150°C, is attributable to the evaporation of physically adsorbed water from the alkali-silicate gel network, in agreement with the well-documented dehydration behavior of sodium silicate hydrates and geopolymer gels [24]. The second, more gradual mass loss extending to approximately 450–500°C with a diffuse endothermic signature, corresponds to the dehydroxylation of silanol (Si–OH) groups and condensation of the remaining silicate network. Importantly, a distinct inflection in the DTA curve consistent with a glass transition (T_g) is observed prior to the onset of the exothermic crystallization event, confirming that the matrix passes through a glassy state during heating. This is a key finding: the presence of a T_g demonstrates that the alkali-activated binder is genuinely glass-forming, and that calcination at 600°C, below the crystallization onset, produces a composite with an amorphous silicate matrix, preserving the ion release kinetics essential for bioactivity [25]. Above 700 °C, an intense exothermic peak appears to be associated with a TG weight increase, seemingly attributable to the onset of SiC oxidation in air.

The XRD patterns of both samples are shown in Figure 2b. The green body (SiCB45S5_AA) presents the characteristic diffraction peaks of *β*-SiC (cubic, space group $F\bar{4}3m$) superimposed on a broad amorphous hump centered at approximately 25–35° 2θ, confirming the glassy nature of the binder phase. After calcination at 600°C (SiCB45S5_600), the *β*-SiC reflections are retained without phase modification, while, interestingly, additional sharp peaks corresponding to combeite ($Na_2Ca_2Si_3O_9$) (trigonal, space group $P3_221$) emerge. Combeite (D phase in Figure 2b) is the primary crystallization product of Bioglass 45S5 emerging after 610°C (the crystallization onset), and its detection confirms that the binder composition is crystallochemically equivalent to that of glass [26]. The observation of this phase below 610 °C indicates that the alkali-activated glassy gel undergoes an earlier crystallization than conventional Bioglass 45S5. Notably, peaks attributable to tricalcium phosphate (TCP, $Ca_3(PO_4)_2$) are also detected in the calcined sample, consistent with the decomposition and crystallization of the sodium calcium phosphate hydrate intermediates formed during processing. TCP is a biocompatible and resorbable calcium phosphate that is known to support osteoblast attachment and can serve as a secondary nucleation site for HA precipitation during SBF exposure [26]. The partial crystallization observed at 600 °C does not necessarily compromise bioactivity, since the crystalline phases present (combeite and TCP) are both intrinsically bioactive, and a substantial amorphous fraction is still detectable in the diffractogram.

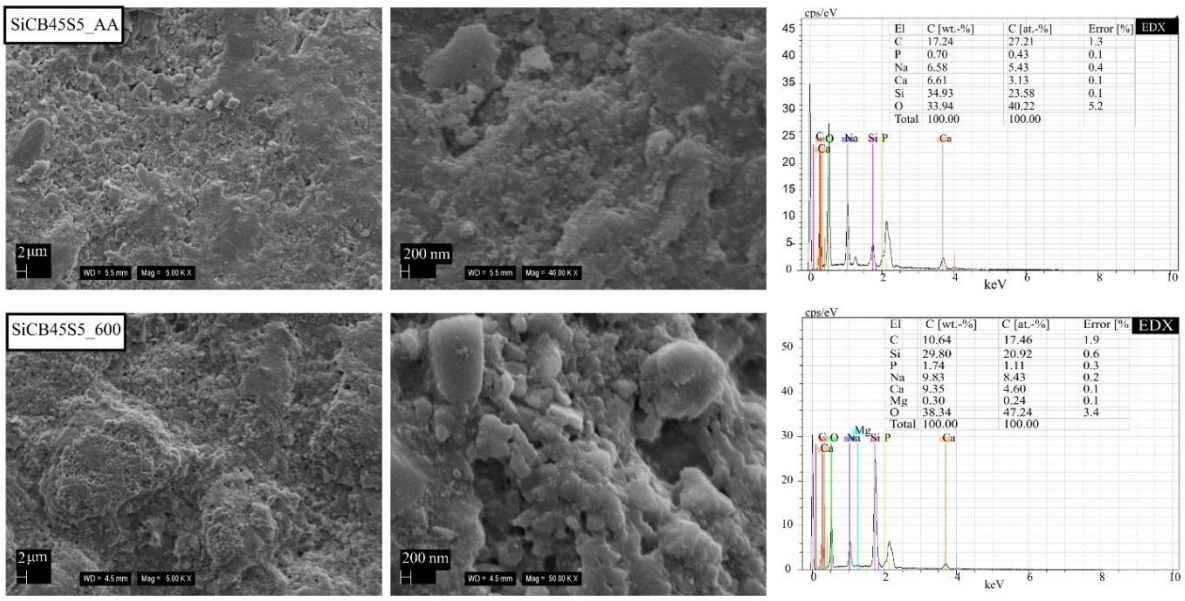

Figure 3. SEM images with two levels of magnification. Top row: alkali-activated green-body (SiCB45S5_AA); bottom row: calcined material (SiCB45S5). Elemental analyses through SEM-EDX spectroscopy are reported on the right-hand side.

The SEM microstructures of SiCB45S5_AA and SiCB45S5_600 at two magnification levels are presented in Figure 3. In the green body (top row), the SiC particles, exhibiting their characteristic polyhedral morphology inherited from the starting powder, are embedded within a continuous, featureless matrix phase. At higher magnification, the matrix in both materials appears homogeneous and dense, without evidence of large pores or phase separation, indicating that the alkali-activated gel has efficiently infiltrated the interparticle spaces and formed a continuous binding network. EDX analysis confirmed that the matrix composition is consistent with the target 45S5 oxide ratios (Si, Na, Ca, and P signals distributed uniformly across the binder phase) with no evidence of compositional segregation at the particle-binder interface. This intimate chemical contact between the SiO_2 shell of SiC and the matrix is a direct consequence of the in-situ alkali-activation mechanism: the silica source is the particle surface itself, ensuring covalent Si–O–Si bonding continuity across the interface [27].
After calcination at 600 °C (bottom row), the overall microstructural homogeneity is preserved. The SiC particles remain well-distributed within the matrix, with no coarsening or agglomeration attributable to the thermal treatment. The matrix exhibits a slightly rougher texture at higher magnification compared to the green body, consistent with the onset of partial crystallization of combeite and TCP identified by XRD (Figure 2b). No evidence of SiC oxidation beyond the pre-existing surface layer, delamination at the particle-matrix interface, or cracking attributable to differential thermal contraction was observed, underlining the chemical and microstructural compatibility of the alkali-activation approach with SiC reinforcement. The preservation of microstructural integrity through the mild calcination step is a key advantage over conventional high-temperature sintering routes, where mismatches in thermal expansion between SiC (4.0×10^{-6} K^{-1}) and bioglass (approximately $12–14 \times 10^{-6}$ K^{-1}) are a major source of interfacial residual stresses and crack initiation [28].

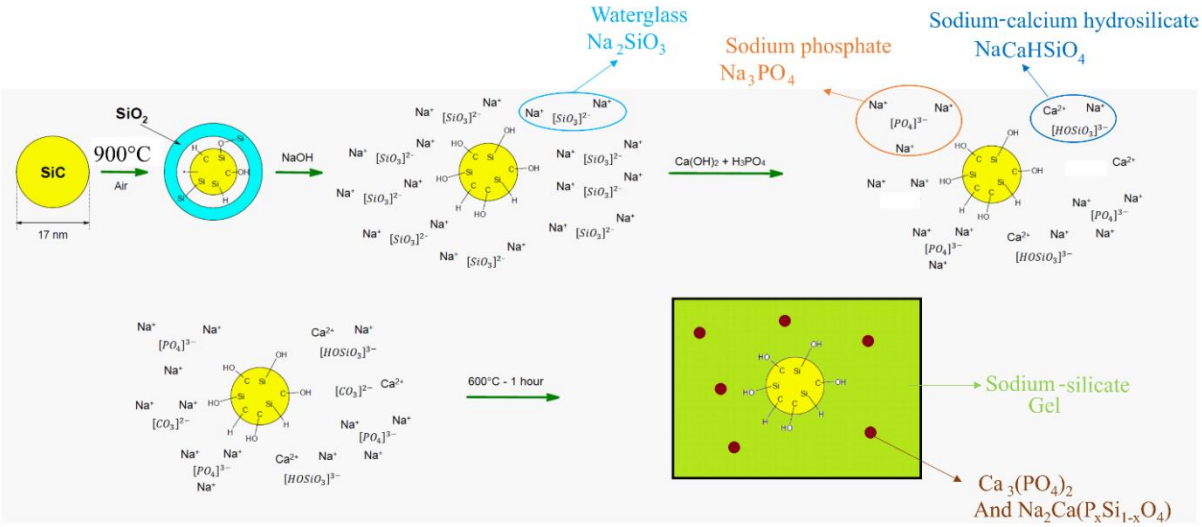

Figure 4. Schematic figure of the reactions underlying the methodological procedure. From the left up: silicon particle before and after calcination at 900 °C; sodium silicate (waterglass – Na_2SiO_3) formation; mixing other ingredients for bioglass precursor and forming sodium phosphate and sodium calcium hydrates; calcination at 600°C, dehydrating and dehydroxylating the hydrates, and formation of combeite and tricalcium phosphate.

The reaction sequence underlying the alkali-activation synthesis is schematically illustrated in Figure 4. In the first step, the pre-calcined SiC particles display a conformal amorphous SiO_2 surface layer. Upon contact with the NaOH solution, this layer undergoes alkaline dissolution according to $SiO_2 + 2NaOH \rightarrow Na_2SiO_3 + H_2O$, forming an in-situ sodium silicate (waterglass) solution. This aqueous sodium silicate acts simultaneously as the reactive binder and as the Si precursor for the final bioglass composition. The subsequent addition of $Ca(OH)_2$ and H_3PO_4 leads to the precipitation of amorphous calcium silicate hydrate and sodium calcium phosphate hydrate intermediates. Upon drying at 150°C, these hydrates set into a rigid green body. The subsequent calcination at 600°C dehydrates and dehydroxylates these intermediates, promoting the partial crystallization of combeite and TCP and consolidating the composite microstructure. The reaction pathway is analogous in spirit to that described by Kokubo for SBF-glass interactions, but proceeding in the opposite direction: here, the alkali-activation chemistry reconstructs the bioglass precursor network in a bottom-up fashion from dissolved silicate species [29].

3.2. Bioactivity test

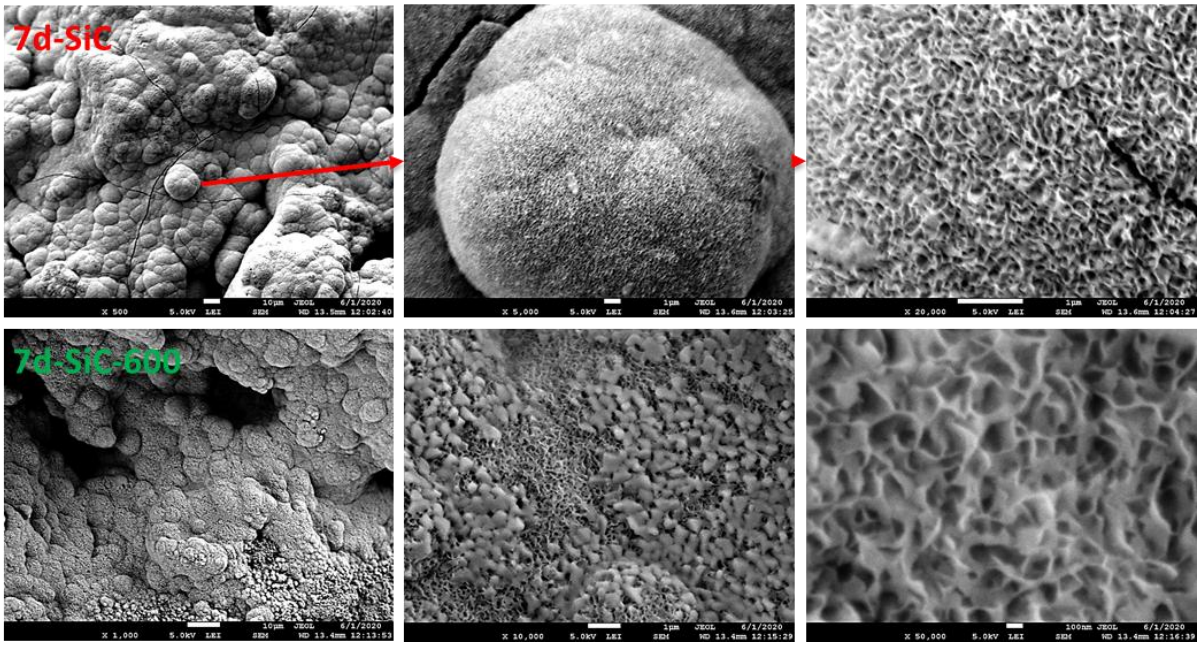

Figure 5. Microstructure analysis through SEM analysis at increasing magnifications (from left to right) of the samples SiCB45S5_AA (top row) and SiCB45S5_600 (bottom row) immersed in SBF for 7 days.

The in vitro bioactivity of both SiCB45S5_AA and SiCB45S5_600 was assessed by immersion in SBF for 7 days. As shown in Figure 5, both samples display extensive surface precipitation after one week. At low magnification, the surfaces are uniformly covered by a new layer of precipitate, and at higher magnification this layer resolves into an assembly of plate- and needle-like crystallites with the characteristic cauliflower morphology of carbonated hydroxyapatite (c-HA) [30]. The c-HA morphology is identical on both samples, indicating that neither the mild calcination treatment nor the partial crystallization of combeite significantly inhibits the bioactivity of the composite. This result is consistent with the thermodynamic argument that combeite, as a network-modified calcium sodium silicate, still presents a high density of non-bridging oxygens at the surface that can exchange with H^+ from SBF solution and initiate the surface dissolution-reprecipitation cascade [31]. The formation of a confluent c-HA layer within 7 days is moreover comparable to the response reported for monolithic 45S5 bioglass in SBF under the same Kokubo protocol [21], confirming that the SiC filler does not act as a bioactivity-blocking diffusion barrier at the composite surface under these conditions. This is a critical distinction from results reported in high-temperature-sintered SiC-glass composites, where thermal degradation of the bioglass and reduced porosity have been shown to extend the induction period for HA nucleation significantly [16]. The presence of SiC particles at the surface may in fact contribute favorably by providing additional silanol groups upon hydration of the SiO_2 shell, which are known to serve as nucleation sites for HA [32].

4. Conclusions

This study introduces a novel, low-temperature alkali-activation method to create SiC-bioglass composites. By using the native SiO_2 layer on SiC particles as a reactive precursor, researchers successfully synthesized a bioactive binder chemically identical to Bioglass 45S5. Pre-calcining β-SiC at 900°C creates a silica surface that, when treated with NaOH, forms an in-situ

sodium silicate binder. This ensures a continuous Si–O–Si covalent bond between the reinforcement and the matrix, preventing the cracking typically seen in traditional sintering. Processing at 600 °C avoids the thermal expansion mismatches and heavy crystallization that usually degrade the performance of ceramic-glass composites. In Simulated Body Fluid (SBF) tests, the composite formed a hydroxyapatite (HA) layer within 7 days. Unlike high-temperature sintered versions, this low-temperature composite maintains bioactivity levels comparable to pure 45S5 bioglass.

Acknowledgements
This work was funded by the EU NextGenerationEU through the Recovery and Resilience Plan for Slovakia under the project No. 09I03-03-V04-00287 and by the project Building-up Centre for advanced materials application of the Slovak Academy of Sciences, ITMS project code 313021T081 supported by the Integrated Infrastructure Operational Programme funded by the ERDF.

References

[1] S.A. Greenwald, S.D. Boden, V.M. Goldberg, Y. Khan, C.T. Laurencin, R.N. Rosier, Bone-graft substitutes: facts, fictions, and applications, J. Bone Joint Surg. Am. 83-A Suppl. 2 (2001) 98–103.
[2] L.L. Hench, Bioceramics: from concept to clinic, J. Am. Ceram. Soc. 74 (1991) 1487–1510.
[3] L.L. Hench, R.J. Splinter, W.C. Allen, T.K. Greenlee, Bonding mechanisms at the interface of ceramic prosthetic materials, J. Biomed. Mater. Res. 5 (1971) 117–141.
[4] O.H. Andersson, K.H. Karlsson, On the bioactivity of silicate glass, J. Non-Cryst. Solids 129 (1991) 145–151.
[5] L.L. Hench, The story of Bioglass, J. Mater. Sci. Mater. Med. 17 (2006) 967–978.
[6] J.R. Jones, Review of bioactive glass: from Hench to hybrids, Acta Biomater. 9 (2013) 4457–4486.
[7] Q.Z. Chen, I.D. Thompson, A.R. Boccaccini, 45S5 Bioglass-derived glass–ceramic scaffolds for bone tissue engineering, Biomaterials 27 (2006) 2414–2425.
[8] A.R. Boccaccini, Q.Z. Chen, L. Lefebvre, L. Gremillard, J. Chevalier, Sintering, crystallisation and biodegradation behaviour of Bioglass®-derived glass–ceramics, Faraday Discuss. 136 (2007) 27–44.
[9] Choyke, W. J., 松波, 弘. & Pensl, G. (2004). Silicon carbide: recent major advances. Springer eBooks.
[10] Bonaventura, G., Iemmolo, R., La Cognata, V., Zimbone, M., La Via, F., Fragalà, M. E., Barcellona, M. L., Pellitteri, R. & Cavallaro, S. (2019). Biocompatibility between Silicon or Silicon Carbide surface and Neural Stem Cells.. Scientific Reports, 9.
[11] Saddow, S., Frewin, C., Coletti, C., Schettini, N., Weeber, E., Oliveros, A. & Jarosezski, M. (2011). Single-Crystal Silicon Carbide: A Biocompatible and Hemocompatible Semiconductor for Advanced Biomedical Applications. undefined.
[12] Fan, J. and Chu, P. (2014). Silicon Carbide Nanostructures: Fabrication, Structure, and Properties. 1st edition, SpringerNature 2014.
[13] M.N. Rahaman, D.E. Day, B. Sonny Bal, Q. Fu, S.B. Jung, L.F. Bonewald, A.P. Tomsia, Bioactive glass in tissue engineering, Acta Biomater. 7 (2011) 2355–2373.
[14] L. Lefebvre, J. Chevalier, L. Gremillard, R. Zenati, G. Thollet, D. Bernache-Assolant, A. Govin, Structural transformations of bioactive glass 45S5 with thermal treatments, Acta Mater. 55 (2007) 3305–3313.
[15] González, P., Serra, J., Liste, S., Chiussi, S., León, B., Perez-Amor, M., Martínez-Fernández, J., de Arellano-López, A. & Varela-Feria, F. M. (2003). New biomorphic SiC ceramics coated with bioactive glass for biomedical applications. Biomaterials, 24(26).
[16] Leenakul, W., Tunkasiri, T., Tongsiri, N., Pengpat, K. & Ruangsuriya, J. (2016). Effect of sintering temperature variations on fabrication of 45S5 bioactive glass-ceramics using rice husk as a source for silica.. Materials Science and Engineering: C, 61.
[17] P. Sepulveda, J.R. Jones, L.L. Hench, Characterization of melt-derived 45S5 and sol-gel-derived 58S bioactive glasses, J. Biomed. Mater. Res. 58 (2001) 734–740.
[18] J.L. Provis, J.S.J. van Deventer (Eds.), Geopolymers: Structure, Processing, Properties and Industrial Applications, Woodhead, Cambridge, 2009.
[19] P. Duxson, A. Fernández-Jiménez, J.L. Provis, G.C. Lukey, A. Palomo, J.S.J. van Deventer, Geopolymer technology: the current state of the art and future research needs, J. Mater. Sci. 42 (2007) 2917–2933.
[20] Sayed, M., Gado, R., Naga, S., Colombo, P. & Elsayed, H. (2020). Influence of the thermal treatment on the characteristics of porous geopolymers as potential biomaterials.. Materials Science and Engineering: C, 116.

[21] T. Kokubo, H. Takadama, How useful is SBF in predicting in vivo bone bioactivity?, Biomaterials 27 (2006) 2907–2915.
[22] Song, Y., Dhar, S., Feldman, L. C., Chung, G. Y. & Williams, J. R. (2004). Modified Deal Grove model for the thermal oxidation of silicon carbide. undefined, 95. https://doi.org/10.1063/1.1690097.
[23] Jepps, N. W. and Page, T. F. (1983). Polytypic transformations in silicon carbide. Progress in Crystal Growth and Characterization, 7(1-4).
[24] J.L. Provis, J.S.J. van Deventer, Geopolymerisation kinetics. 2. Reaction kinetic modelling, Chem. Eng. Sci. 62 (2007) 2318–2329.
[25] L.L. Hench, D.E. Clark, Physical chemistry of glass surfaces, J. Non-Cryst. Solids 28 (1978) 83–105.
[26] R.Z. LeGeros, Calcium phosphates in oral biology and medicine, Monogr. Oral Sci. 15 (1991) 1–201.
[27] P. Duxson, J.L. Provis, G.C. Lukey, F. Separovic, J.S.J. van Deventer, ^{29}Si NMR study of structural ordering in aluminosilicate geopolymer gels, Langmuir 21 (2005) 3028–3036.
[28] ElBatal, H. A., Azooz, M., Khalil, E. M. A., Monem, A. S. & Hamdy, Y. (2003). Characterization of some bioglass–ceramics. Materials Chemistry and Physics.
[29] T. Kokubo, H. Kushitani, S. Sakka, T. Kitsugi, T. Yamamuro, Solutions able to reproduce in vivo surface-structure changes in bioactive glass-ceramic A-W, J. Biomed. Mater. Res. 24 (1990) 721–734.
[30] C. Rey, C. Combes, C. Drouet, H. Sfihi, A. Barroug, Physico-chemical properties of nanocrystalline apatites: implications for biominerals and biomaterials, Mater. Sci. Eng. C 27 (2007) 198–205.
[31] L.L. Hench, J. Wilson (Eds.), An Introduction to Bioceramics, World Scientific, Singapore, 1993.
[32] A. Oyane, H.M. Kim, T. Furuya, T. Kokubo, T. Miyazaki, T. Nakamura, Preparation and assessment of revised simulated body fluids, J. Biomed. Mater. Res. A 65 (2003) 188–195.